J. Mol. Model. **1997**, *3*, 156 – 171

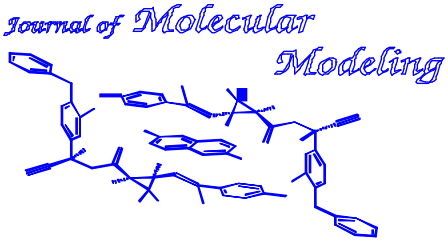

Critical Point Analysis of Calculated Electron Density Maps at Medium Resolution: Application to Shape Analysis of Zeolite-Like Systems

Laurence Leherte* and Daniel P. Vercauteren

Laboratoire de Physico-Chimie Informatique, Institute for Studies in Interface Sciences (ISIS), Facultés Universitaires Notre-Dame de la Paix, Rue de Bruxelles 61, B-5000 Namur, Belgium ; Tel.: +32-81-724560; Fax.: +32-81-724530 (leherte@scf.fundp.ac.be, vercau@scf.fundp.ac.be)

Received: 10 January 1997 / Accepted: 21 March 1997 / Published: 3 April 1997

Abstract

A method, derived from the procedure implemented in the program ORCRIT which was originally developed by C.K. Johnson, is presented for the topological analysis of zeolite electron density maps. This method is an approach to shape analysis of zeolitic frameworks through the location, identification, and linkage of critical points (points where the gradient of the density vanishes) in medium resolution electron density maps. It is observed that, at 3 Å resolution, tetrahedral sites and oxygen atoms generate peaks (density maxima) and passes (saddle points), respectively. The definition of ellipsoids, built at each peak location from their three local density curvatures, is used to generate a void volume wherein atomic or molecular probes can interact. The energetic behaviour of probes of several sizes interacting with ferrierite and mordenite is qualitatively studied through a pseudo- Lennard-Jones potential approximation.

Keywords: critical point analysis, shape analysis, electron density map, ferrierite, mordenite

Introduction

The modeling of molecular recognition phenomena within large biomolecular or material systems often calls for shape analysis approaches which can match the external surface of the host structure *versus* its receptor. The most common molecular surface representations, which do not involve any probe element, are based on the well-known van der Waals (vdW) representation wherein spheres are centred at atom locations, or on electron iso-density contours. On the other hand, when interaction concepts with the surroundings need to be considered, solvent accessible surfaces and molecular electrostatic potentials are often used.

The matching of two molecular structures may be a tedious task when accuracy is needed, especially if the method that is used requires the alignment of both partners through a succession of translation-rotation movements of three-dimensional properties such as electron density distributions and molecular electrostatic potential maps. In such a case, a first guess of the translation-rotation operation is helpful to reduce the number of unsuccessful trials. For example, Norel *et al.* [1] applied a technique borrowed from the computer vision discipline, the geometric hashing paradigm, to receptor-ligand recognition and docking. In their approach, sets of

* *To whom correspondence should be addressed*

three atoms are selected from the ligand structure and matched against similar sets defined for the receptor. When distance constraints are satisfied, the triangles are stored in a so-called hash table. The storage address is computed from the lengths of sides of the triangles. The authors also compared their approach to several other geometrically-based methods applied to molecular docking.

The need of an alignment procedure can actually be overcome by avoiding an explicit reference to atom or grid positions, and by a reduction of the number of representation data. These two aspects are prominent in topology-based approaches. In this sense, major achievements were carried out by Mezey in the particular fields of molecular shape characterization and molecular similarity. Within his Shape Group Method (SGM), various surface representations such as vdW surfaces, molecular iso-density contours (MIDCO), molecular electrostatic potential (MEP) iso-contours, or even molecular orbitals (MO) can be described using tools of topology [2]. The local curvature properties of such contours are characterized by the eigenvalues of two by two Hessian matrices $\mathbf{H}(\mathbf{r})$ defined at each point $\mathbf{r}$ on the contour surface within local tangent planes. Points with zero, one, and two negative eigenvalues of $\mathbf{H}(\mathbf{r})$ belong to domains that are locally concave, of the saddle type, and convex, respectively. A molecular surface is thus partitioned into domains whose specific arrangement is described in terms of homology groups characterized by their ranks, or Betti numbers [3]. The Betti numbers are topological invariants and may thus serve as a basis for comparing shapes of different molecules [4].

Domain decomposition of Connolly surfaces in terms of convex, saddle-shaped, and concave faces, were also carried out by Lin *et al.* [5]. In their method, the authors reduce each face of the solvent accessible surface in terms of a critical point. The resulting representation consists of a limited number of points disposed at key locations on the surface. Topological representations are therefore independent of the geometrical parameters such as atom locations, bond distances and angles.

Another aspect of the topological approaches relies in the three-dimensional analysis of electron density (ED) distributions and molecular electrostatic potential (MEP) maps. According to Bader [6], the topological properties of ED scalar fields can conveniently be summarized in terms of the number and kind of their critical points, *i.e.*, points where the gradient of the density is equal to zero. Each critical point can be identified by its corresponding three by three Hessian matrix $\mathbf{H}(\mathbf{r})$ which is built on the local second derivatives of the ED function. In Bader's theory of atoms in molecules (AIM), each atom is associated with an attractor and its basin bounded by a zero-flux surface over which many atomic properties can be integrated. This yields a unique partitioning of a total system into a set of bounded spatial regions. The critical points are then linked through a gradient vector field analysis to generate a graph whose vertices and edges are critical points and gradient trajectories, respectively.

Similarily to Bader's approach, C.K. Johnson [7] developed a critical point analysis method, based on Morse theory, for the location, identification, and connection of critical point trees within experimental protein electron density maps. His method was aimed at the automated interpretation of X-ray diffraction data for protein structures. In a related philosophy of working, Greer [8] designed a skeletonization approach for the visual interpretation of protein ED maps. His approach is now implemented in the well-known FRODO and O programs [9]. Because the interpretation of protein maps may still be a tedious task, which requires much expertise and visual manipulation, we have chosen to pursue Johnson's work, in the frame of the Molecular Scene Analysis (MSA) project, to integrate his method in an automated approach for the resolution of protein electron density maps [10-12].

MEP functions have also been the subject of topological analysis studies [13-14]. As, by definition, critical points correspond to points where the gradient of the electrostatic potential vanishes $\nabla V = 0$, they also correspond to locations where the electrostatic field is exactly zero. In a brute force approach, the locations and connections of extrema in MEP were carried out by Willett and coworkers [15-16] in order to generate the so-called field-graphs. In their approach, grid points with MEP values ranging below or beyond given cut-off values are merged into single points which are further connected depending upon their closeness. Such graph representations facilitate the alignment of MEP fields during a similarity-search procedure through a maximal common subgraph isomorphism algorithm. This is particularly important for the similarity searching in large data bank where speed and efficiency are always simultaneously required.

Finally, regardless of topological analysis methods, other approaches have been used to simplify the representation of 3D maps and consequently increase the speed of docking algorithms. Several authors developed a procedure to fit Gaussian functions to MEP [17] and ED functions [18-21] and, by that way, increase the speed of shape similarity evaluation through the use of the Carbo similarity index [17-19, 21-22].

In the present paper, we describe a topological analysis method based on the ORCRIT approach [7] for applications to critical point analysis of zeolite electron density maps at medium resolution. A numerical procedure is derived for the shape reconstruction of zeolitic frameworks, and the evaluation of pseudo-interaction energy values between the framework and a probe molecule. In the next section, we present all mathematical aspects related to the critical point analysis and the pseudo-interaction energy determination. Applications to ferrierite- and mordenite-type frameworks interacting with probes of different sizes are then presented, and first comparisons are carried out with conventional energy calculations [23].

Methodology

In this section, the critical point analysis approach as implemented in ORCRIT [7] is presented. It more particularly shows how critical points are defined and connected to generate graph representations and shape reconstructions.

Critical point analysis

An electron density (ED) distribution $\rho(\mathbf{r})$ can be described in terms of the location and identification of its critical points, *i.e.*, points where the gradient (∇) of the density is equal to zero. They are thus characterized as maxima, minima, or saddle points depending upon the sign of the second derivatives of $\rho(\mathbf{r})$. The Hessian matrix ($\mathbf{H}$) of a continuous 3D function such as the ED is built from its second derivatives:

$$\mathbf{H}(\mathbf{r}) = \begin{pmatrix} \frac{\partial^2}{\partial x^2}\rho & \frac{\partial^2}{\partial x \partial y}\rho & \frac{\partial^2}{\partial x \partial z}\rho \\ \frac{\partial^2}{\partial y \partial x}\rho & \frac{\partial^2}{\partial y^2}\rho & \frac{\partial^2}{\partial y \partial z}\rho \\ \frac{\partial^2}{\partial z \partial x}\rho & \frac{\partial^2}{\partial z \partial y}\rho & \frac{\partial^2}{\partial z^2}\rho \end{pmatrix} \quad (1)$$

This real and symmetric matrix can be diagonalized. The three resulting eigenvalues provide informations relative to the local curvature; the Laplacian, which is the summation over the three eigenvalues, gives details about the local concentration (sign < 0) or depletion (sign > 0) of the electron density. If the rank (number of non-zero eigenvalues) of the diagonalized matrix is 3, then four cases are met. The signature (sum of the sign of the eigenvalues) $s = -3$ corresponds to a local maximum or *peak*, *i.e.*, the electron density function adopts maximum values along each of the three principal directions x', y', and z'; $s = -1$ corresponds to a saddle point or *pass* where two of the eigenvalues are negative; $s = +1$ corresponds to a saddle point or *pale* characterized by only one negative eigenvalue, and $s = +3$ corresponds to a local minimum or *pit*, *i.e.*, the electron density function adopts minimum values along each of the three principal directions.

Morse theory allows to determine whether the set of critical points is topologically consistent. It is applicable to functions which are everywhere twice differentiable, and wherein there is no degenerate critical points, *i.e.*, no zero eigenvalues of the Hessian matrix at the critical point locations. Considering M_k as the number of critical points with index *k* of the function $\rho(\mathbf{r})$, then [24]:

$$M_3 - M_2 + M_1 - M_0 = 1 \quad (2)$$

where M_3, M_2, M_1, and M_0 stand for the number of peaks, passes, pales, and pits, respectively.

In the case of crystals, the critical point network is defined not only by the molecular structure but also by the lattice periodicity and the space group symmetry. Due to periodic boundary conditions, a unit cell can be considered as a 3D torus, each pair of opposite faces being connected. This means that the motif of critical points is not isolated but interacts with its periodic images and, therefore, the number of critical points is constrained by the relationship:

$$M_3 - M_2 + M_1 - M_0 = 0 \quad (3)$$

At atomic resolution, peaks and passes are normally associated with the presence of atoms and chemical bonds, respectively, while pales and pits occur as a result of the geometrical arrangement of the atoms and the corresponding networks of bonds. Pales and pits are found in the interior of rings and cages, respectively [6].

Our program uses a two-pass approach to detect critical points in an electron density map. During the first pass, each grid point whose density value is larger or equal to a selected minimum value, ρ_{min}, is considered as the central point of a 27 grid point subset, which includes its 26 nearest neighbours. The method looks, in particular, at the electron density differences between adjacent points and at patterns of increasing or decreasing electron density values within grid planes to assess whether the central point might be close to a peak, a pass, a pale or a pit. When a possible critical point is found, its coordinates (x, y, z) are estimated using a linear interpolation procedure. In the second pass, a more refined procedure is used. It is based on a three-dimensional linear-blending calculation which uses the numerical density map stored as a three-dimensional table. In order to find local critical points, 32 coefficients, *i.e.*, a 3D pattern of 32 adjacent density points, are needed [25]. All critical point search algorithms that were implemented in ORCRIT were kept since they are well suited for the analysis of a 3D grid. For the present work, we however modified the ORCRIT program in

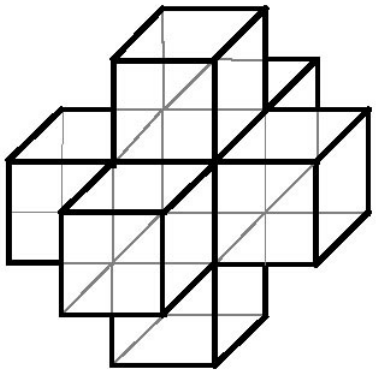

Figure 1. *32-point grid pattern for the refinement of critical point coordinates, density, and eigenvalues.*

order to consider any grid size, and to increase the numerical precision level.

Figure 1 depicts a subset of 32 connected grid points taken from a global electron density map. This subset includes the number of degrees of freedom needed for the three-dimensional polynomial fit as expressed by:

$$\rho(x,y,z) = \sum_{i=0}^{1}\sum_{j=0}^{1}\sum_{k=0}^{1} a_{ijk}x^i y^j z^k + \sum_{i=0}^{1}\sum_{j=0}^{1}\sum_{k=2}^{3} a_{ijk}x^i y^j z^k + \sum_{i=0}^{1}\sum_{j=2}^{3}\sum_{k=0}^{1} a_{ijk}x^i y^j z^k + \sum_{i=2}^{3}\sum_{j=0}^{1}\sum_{k=0}^{1} a_{ijk}x^i y^j z^k \quad (4)$$

Equation (4) and its derivatives allow the determination of the density value at a given point **r** = (x, y, z), as well as of its first and second derivatives, *i.e.*, $\nabla\rho(\mathbf{r})$ and **H**(**r**). The coefficients a_{ijk} are determined by considering equation (4) as a Lagrangian linearly blended interpolation polynomial. The coordinates of any critical point identified in the first pass are refined by iteratively applying equation (5) and the equation:

$$\mathbf{r}_{new} = \mathbf{H}^{-1}(\mathbf{r})\cdot\nabla\rho(\mathbf{r}) \quad (5)$$

The procedure terminates when the difference ($\mathbf{r}_{new} - \mathbf{r}$) is close to a predetermined value, which is set to 0.0005 (in grid units). Once **H** has been determined, the eigenvalues and eigenvectors are obtained by using a QR algorithm [26]. For each individual critical point, the three eigenvectors reflect the three main axis of the local electron density function, along which the eigenvalues are established. The column arrangement of the three orthonormal eigenvectors in a three by three matrix representation corresponds to the actual transformation matrix **U** needed to diagonalize **H** according to:

$$\mathbf{H'}(\mathbf{r}) = \mathbf{U}^T\,\mathbf{H}(\mathbf{r})\,\mathbf{U} \quad (6)$$

The characteristics of nearby critical points - types, distances, density heights, eigenvector projections - are used in order to derive a weight function for possible connections. In particular, such a function is used in a graph theoretical approach for representing the full network of critical points. In graph theory, a graph is a representation of a finite set of points (or vertices) and their connectivity, *i.e.*, the corresponding set of edges. In particular, a connected graph consists in a set of vertices in which any pair may be connected by a path formed by one or several successive edges in the graph. Many connected graphs contain rings of points and edges (circuits). The weight of a connection between two critical points, w_{ij}, as calculated in the original version of ORCRIT, is inversely proportional to its occurrence probability. The

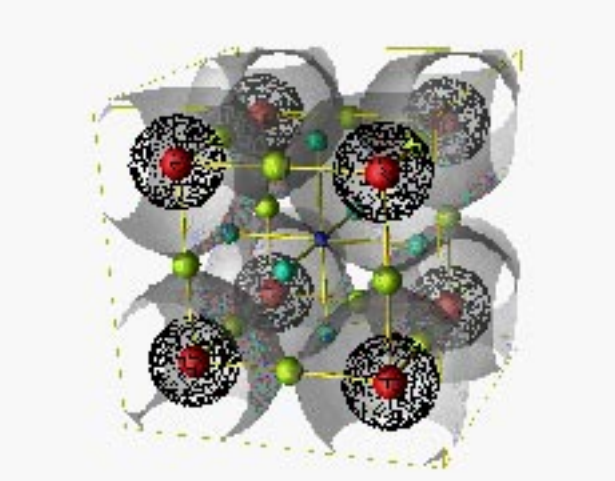

Figure 2. *Critical point networks 'peak (red)-pass (yellow)' and 'pit (dark blue)-pale (light blue)' of a cubic arrangement of three-dimensional Gaussian functions.*

weight w_{ij} of any pair of critical points is computed according to the following equation:

$$w_{ij} = \Delta r\ R\ F \quad \text{where} \quad R = \frac{1+\dfrac{|\Delta\rho|}{\rho_i+\rho_j}}{\sqrt{\rho_i+\rho_j}} \quad (7)$$

Δr being the distance between the two critical points, $|\Delta\rho|$ being the absolute value of the density difference ($\rho_i - \rho_j$), and F being equal to ($3 - F_1 - F_2$), where F_i denotes the normalized projection of the eigenvector of point i along the vector $\Delta\mathbf{r}$ connecting the two critical points. The original ORCRIT program is coded so as to build minimal spanning trees (graphs without any closed path) and connections between critical points of the same kind are accepted. In the revised version of the program, we first allow for circuits, and we added a constraint which prevents critical points of the same type to be connected. Figure 2 represents a cubic network of critical points, with one peak located at each of the 8 corners. The 8 Gaussian functions built on these peaks generate a pass on each of the edges, pales centred on the 6 faces, and one pit located in the centre of this cube. To generate this figure, a maximal cutoff value for F was set equal to ($3 - \cos30° - \cos30°$).

Shape reconstruction

At the critical point locations, the three main curvatures of the electron density function are the eigenvalues of the Hessian matrix constructed from the second derivatives. It is assumed that this local information can be transferred to the space surrounding the critical point concerned; hence it is

possible to evaluate (or reconstruct) the 3D function in the close neighbourhood of each point. Each maximum of the electron density function, *i.e.*, each peak, is considered as the centre of expansion of a Gaussian function and such a mathematical expression is fitted in order to define a volume around each peak taking into account its three characteristic eigenvalues:

$$\rho(\mathbf{r}) = \rho(0) e^{\frac{\alpha \mathbf{r}^T \mathbf{H}' \mathbf{r}}{\rho(0)}} \tag{8}$$

where **H'** is the diagonalized form of **H**, and **r** is defined in a reference frame built on the three corresponding eigenvectors. In the frame of ORCRIT, the parameter α is set equal to 2.0. In order to evaluate the volume associated with a particular peak, the exponential term of the Gaussian function has been integrated over the space within the frame of the ellipsoid:

$$\int_V e^{\frac{\alpha \mathbf{r}^T \mathbf{H}' \mathbf{r}}{\rho(0)}} d\mathbf{r} \tag{9}$$

which leads to the definition of an ellipsoid characterized by three main axes r_X, r_Y, and r_Z:

$$V = \frac{\pi^{3/2} \rho(0)^{3/2}}{2^{3/2} |h_x|^{1/2} |h_y|^{1/2} |h_z|^{1/2}} = \frac{4\pi}{3} r_x r_y r_z \tag{10}$$

and hence provides a method of representing shape anisotropy of the critical points. This shape description is extended to a whole molecule by considering a set of ellipsoids, and a descriptor for this structure is defined in terms of interaction energy values. The total interaction energy E between the host ellipsoids and a probe is expressed within a pseudo-pair-potential approximation, wherein the dispersive interaction between an ellipsoid i and a sphere j is proportional to their volume product:

$$E = \sum_{i<j} E_{ij} \tag{11}$$

$$E_{ij} = -A_{ij}/r_{ij}^{6} + B_{ij}/r_{ij}^{12}$$

$$\text{where } A_{ij} > 0 \text{ and } B_{ij} > 0 \tag{12}$$

$$A_{ij} = V_i \cdot V_j \tag{13}$$

$$B_{ij} = A_{ij} (r_i + r_j)^6 \tag{14}$$

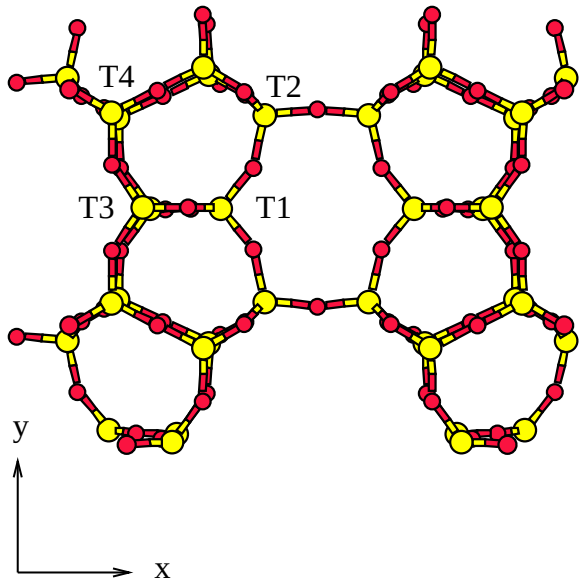

Figure 3. *Crystallographic structure of ferrierite (one unit cell) retrieved from the MSI Technologies data bank (Si: yellow, O: red).*

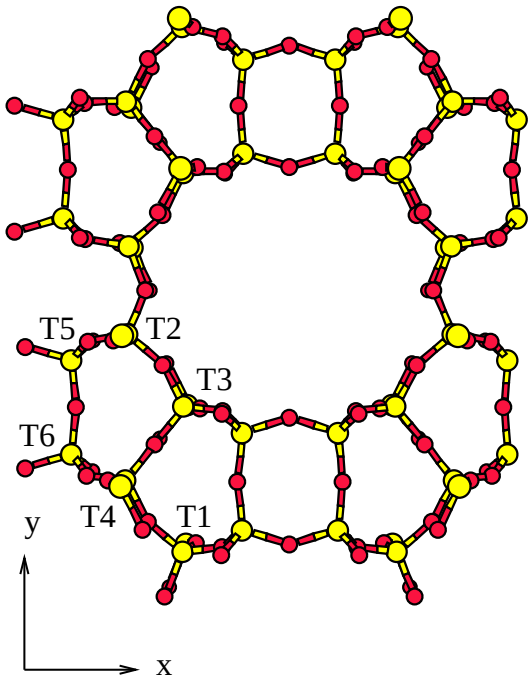

Figure 4. *Crystallographic structure of mordenite (one unit cell) retrieved from the MSI Technologies data bank (Si: yellow, O: red).*

Table 1. *Ferrierite (FER) and mordenite (MOR) electron density map specifications used for topological analyses at 3 Å resolution.*

	FER	MOR
Unit cell parameters	19.156	18.094
(Å and degrees)	14.127	20.516
	7.489	7.524
	90.00	90.00
	90.00	90.00
	90.00	90.00
Space group	Immm	Cmc21
Channel system	10-T [001]	12-T [001]
	8-T [010]	8-T [010]
Unit cell content	$Si_{36}O_{72}$	$Si_{48}O_{96}$
Grid intervals (Å)	0.171	0.162
	0.126	0.183
	0.117	0.118

Table 2. *Critical point properties (electron density ρ, eigenvalues h, and distance versus the atom position d(cp-at)) of the ferrierite electron density map at 3 Å resolution.*

	ρ ($e^-/Å^3$)	h ($e^-/gu^2 \cdot Å^3$) [a]			d(cp-at) (Å)
T1	3.30	-0.018	-0.016	-0.013	0.02
T2	2.77	-0.019	-0.010	-0.008	0.27
T3	3.11	-0.020	-0.014	-0.009	0.32
T4	2.99	-0.017	-0.015	-0.008	0.16
O1	1.60	-0.012	-0.007	0.014	0.08
O2	2.22	-0.012	-0.007	0.014	0.30
O3	1.77	-0.024	-0.016	0.008	0.30
O4	1.78	-0.016	-0.012	0.015	0.36
O5	2.22	-0.023	-0.012	0.011	0.00
O6	2.04	-0.021	-0.010	0.011	0.33
O7	2.13	-0.022	-0.011	0.009	0.26
O8	2.09	-0.023	-0.015	0.007	0.22

[a] gu = "grid unit", i.e., *grid interval.*

Table 3. *Critical point properties (electron density ρ, eigenvalues h, and distance versus the atom position d(cp-at)) of the mordenite electron density map at 3 Å resolution.*

	ρ ($e^-/Å^3$)	h ($e^-/gu^2 \cdot Å^3$) [a]			d(cp-at) (Å)
T1	2.87	-0.018	-0.015	-0.011	0.09
T2	2.87	-0.018	-0.015	-0.011	0.09
T3	2.92	-0.018	-0.016	-0.012	0.13
T4	2.92	-0.018	-0.016	-0.012	0.13
T5	2.97	-0.020	-0.018	-0.011	0.06
T6	2.89	-0.021	-0.014	-0.011	0.06
O1	2.14	-0.023	-0.018	0.008	0.33
O2	2.14	-0.023	-0.018	0.008	0.33
O3	2.12	-0.020	-0.018	0.009	0.33
O4	2.12	-0.020	-0.018	0.009	0.33
O5	1.94	-0.020	-0.016	0.012	0.23
O6	1.94	-0.019	-0.016	0.012	0.23
O7	2.05	-0.024	-0.016	0.013	0.31
O8	2.28	-0.027	-0.017	0.008	0.29
O9	1.97	-0.026	-0.015	0.011	0.46
O10	2.00	-0.020	-0.013	0.013	0.33
O11	1.90	-0.023	-0.015	0.014	0.12
O12	1.64	-0.015	-0.011	0.013	0.01
O13	1.53	-0.015	-0.012	0.016	0.51

[a] gu = "grid unit", i.e., *grid interval.*

r_{ij} being the separation distance between particles i and j, and r_i and r_j, their radii calculated along the interdistance vector i-j. In such a formula, it is considered that the equilibrium distance between i and j is given by $2^{1/6}(r_i + r_j)$ and $E_{ij} = 0$ when $r_{ij} = (r_i + r_j)$. The idea of using a pseudo-potential energy function in order to determine the optimal steric location of a guest molecule was also developed by Kuntz and coworkers [27-29] in the program DOCK. These authors simplified the overlap energy between two molecules to a contribution depending upon the vdW radii of the interacting atoms and their separation distance. However, considering a Lennard-Jones type potential allows us to emphasize the effect of global curvature of the neighbourhood, *e.g.*, a cavity leading to more attractive energies.

Fitting Gaussian functions to a higher resolution representation, *i.e.*, to atoms, has been done latter by Grant and Pickup [20] to overcome the limitations of hard sphere representations of molecular shapes. From such functions, these authors were able to derive gradients and Hessian of the nu-

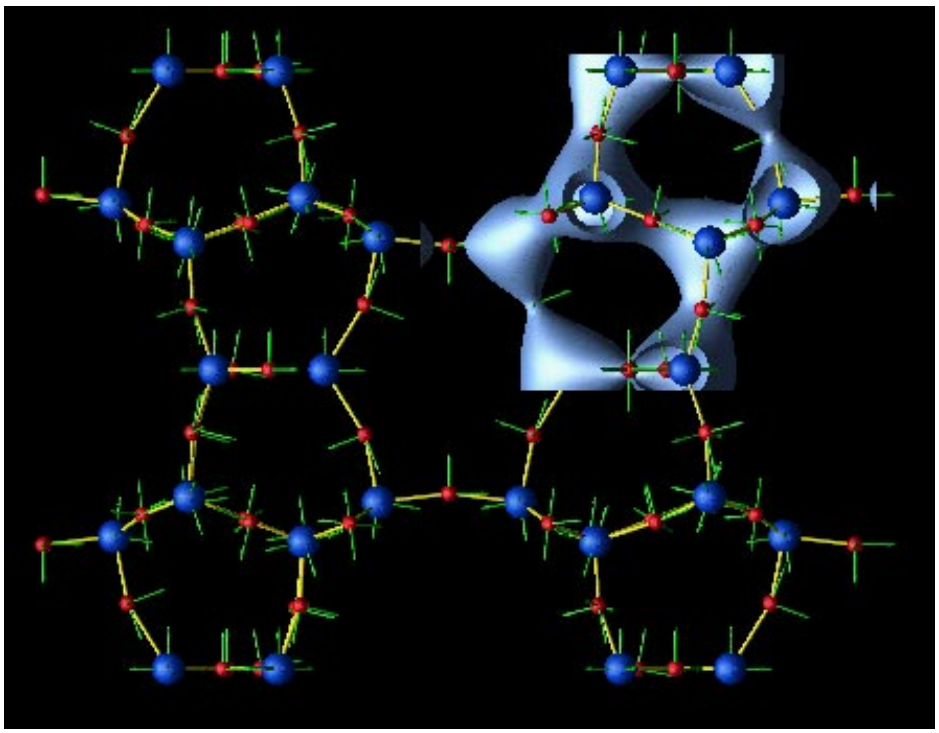

Figure 5. *Framework of critical points (peaks in blue and passes in purple), eigenvectors (green arrows), and iso-electron density contour (1.7 $e^-/Å^3$) obtained from the topological analysis of the ferrierite electron density map at 3 Å resolution. The critical point linkage is shown using yellow sticks.*

clear coordinate derivatives, *i.e.*, properties similar to critical point characteristics.

Applications to shape analysis of ferrierite and mordenite

In this section, we describe applications of our critical point analysis program to two zeolitic frameworks, ferrierite and mordenite. Zeolites are crystalline alumino-silicates characterized by the presence of pores and cavities wherin guest molecules can diffuse and interact. Consequently, zeolites and related materials are presently one of the most technologically important classes of inorganic compounds in numerous industrial processes. Examples comprise applications as catalysts, selective adsorbants, ion exchangers as well as shape-selective molecular sieves. Confinement is one of their leading aspects [30-32]. Molecules in zeolites are considered as solvated by the surrounding framework, which implies favourable interactions between the host network and the guest molecule. The topology of the zeolite network is thus deeply involved in confinement effects.

Crystallographic structures of ferrierite (Figure 3) and mordenite (Figure 4) were retrieved from the MSI Technologies data bank [33] and used as input to the program XTAL [34] to generate the corresponding electron density maps (EDMs). Both ferrierite and mordenite structures are characterized by a network of channels running along the crystallographic axes c [001] and b [010]. Grid specifications of the EDMs are reported in Table 1. We selected a resolution of 3 Å ($\sin\Theta/\lambda = 0.167$) following the work previously done on the shape complementarity analysis of drug

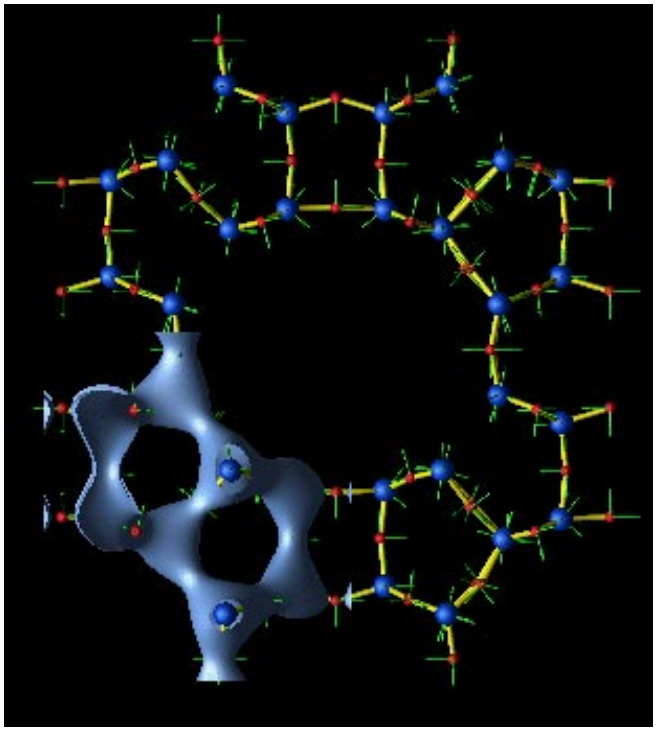

Figure 6. *Framework of critical points (peaks in blue and passes in purple), eigenvectors (green arrows), and iso-electron density contour (1.7 $e^-/Å^3$) obtained from the topological analysis of the mordenite electron density map at 3 Å resolution. The critical point linkage is shown using yellow sticks.*

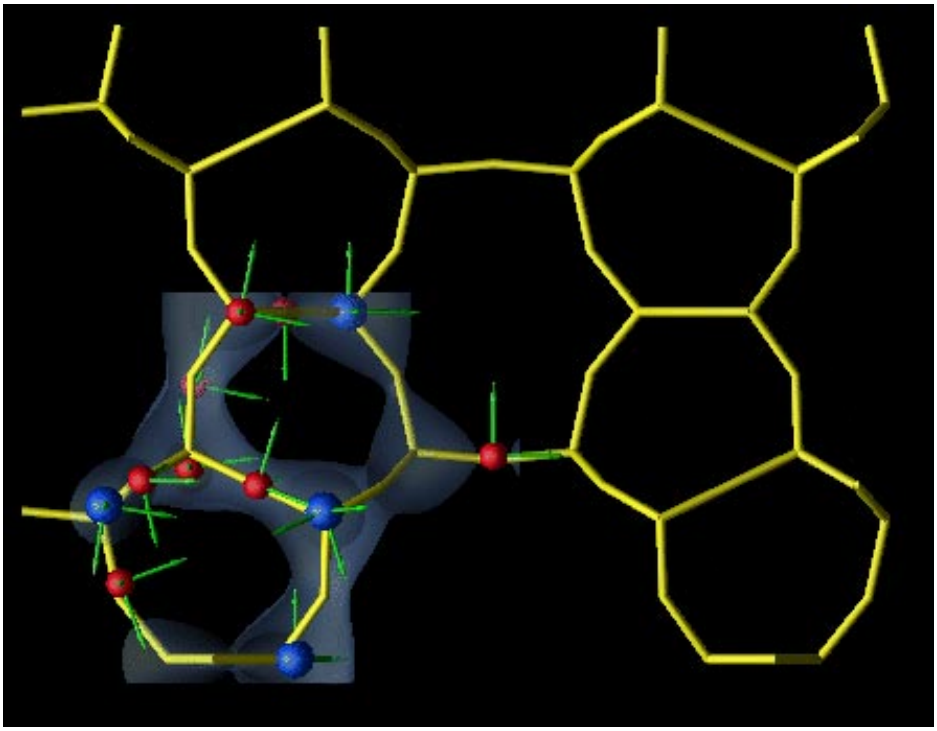

Figure 7. *Critical points for an asymmetric motif Si_4O_8 (peaks in blue and passes in purple), eigenvectors (green arrows), and iso-electron density contour (1.7 $e^-/Å^3$) obtained from the topological analysis of the ferrierite electron density map at 3 Å resolution. The results are superimposed onto the crystallographic structure (yellow sticks) retrieved from the MSI Technologies data bank.*

molecules within confined receptors such as DNA [35] and β-cyclodextrin [36-37].

In both cases, the unit cell was divided into 112 x 112 x 48 grid points. Since symmetry operations and periodicity are explicitly taken into account in the topological and shape analysis programs, calculations were carried out with one asymmetric unit only. The maximal electron density values that were obtained are equal to 3.30 and 2.97 $e^-/Å^3$ for ferrierite and mordenite, respectively.

Critical point analysis results

A minimal density cutoff value was set equal to 1.50 $e^-/Å^3$ in order to avoid the generation of peaks and passes originating from ripples due to the Fast Fourier Transform approximations when generating EDMs using the program XTAL. Under such conditions, pales and pits cannot be detected, and we will focus on the analysis of highest density critical points only.

The application of the critical point analysis method generated, very interestingly, peaks located at the tetrahedral site positions, and passes close to the zeolite oxygen atoms (Tables 2 and 3). Figures 5 and 6 depict the location of the critical points (peaks in blue and passes in purple) in the electron density map of ferrierite and mordenite at 3 Å resolution, respectively. The orientation of their three eigenvectors is shown using green arrows. It was actually observed that such a topological behaviour is valid at resolution values ranging from 2.1 to 3.5 Å. At higher resolutions, peaks tend to appear at oxygen atom positions, as observed at atomic resolution, while at lower resolutions, the number of discovered critical points becomes very low.

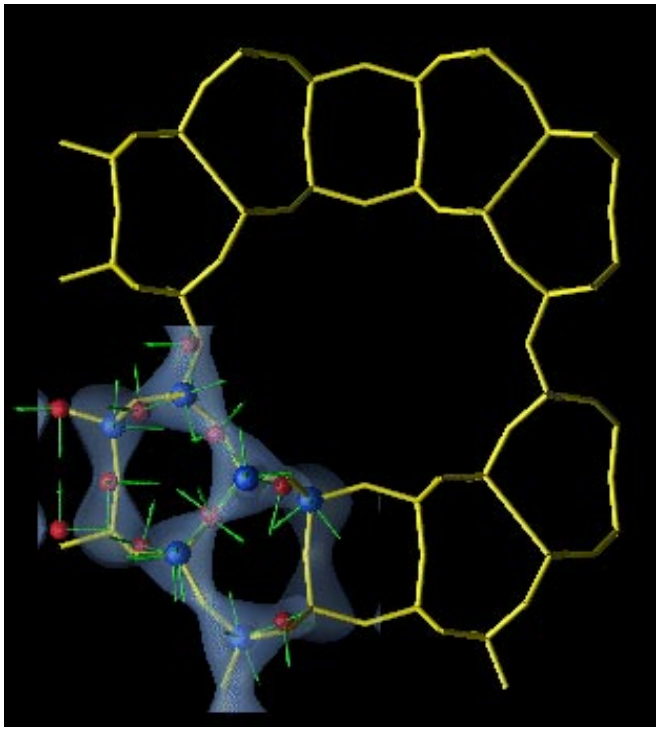

Figure 8. *Critical points for an asymmetric motif Si_6O_{13} (peaks in blue and passes in purple), eigenvectors (green arrows), and iso-electron density contour (1.7 $e^-/Å^3$) obtained from the topological analysis of the mordenite electron density map at 3 Å resolution. The results are superimposed onto the crystallographic structure (yellow sticks) retrieved from the MSI Technologies data bank.*

We must point out here that, in our topology-based model, large size elements (ellipsoids) are centred on the Si atoms. This is due to the fact that electron density distributions are computed through a Fourier Transform of calculated structure factors. These structure factors are built from atomic scattering factors whose contributions are generated both by the core and valence electrons. Thus, since Si atoms have a higher atomic number than O atoms, their scattering power is increased, and they generate higher density values.

The distances d(cp-at) between the critical points and the actual atom locations range between 0.02 and 0.51 Å. In general, peaks are closer to their respective T-site than passes are to their corresponding oxygen atom. Passes are located on a straight line joining their two neighbouring peaks (Figures 7 and 8), *i.e.*, a path slightly different from the bended Si-O-Si linkage pattern.

It is also interesting to analyze the 3D orientation of the ellipsoids, *i.e.*, the direction of the critical point eigenvectors. For each individual critical point, the three eigenvectors reflect the three main axis of the local electron density function, along which the eigenvalues are established. Matrices **U** defined in equation (6) are given in Table 4 for all peaks found in the electron density maps of both zeolite structures at 3 Å resolution. It is first observed that the ellipsoid orientation is consistent with the local symmetry of the zeolitic framework. In the case of ferrierite, the three eigenvectors associated with site T1 belong to two mirror planes. Indeed, the analysis of **U** given in Table 4 shows that the three eigenvectors have a major component directed along one direction, z (or crystallographic axis c) for the first eigenvector, x (or a) for the second eigenvector, and y (or b) for the third eigenvector. Regarding T2 and T3, one eigenvector has its major component pointing along one specific direction, z and y, respectively; while the two others lie in a plane perpendicular to that direction. Site T4 has no particular orientation. These observations should also be related to the multiplicity of each of these sites. T1, T2, T3, and T4 have a multiplicity of 1/4, 1/2, 1/2, and 1, respectively. They are located at particular crystallographic positions, *i.e.*, on symmetry elements. The lower the multiplicity is, the higher the degree of alignement of the ellipsoid with the crystallographic axes is. In the case of mordenite, all T-sites have a multiplicity of 1. The orientation of the eigenvectors should thus be related to their local symmetry only. For example, sites T3 and T4 both have their third eigenvector that is strongly aligned with z, while the other two eigenvectors are arranged according to the local bonding pattern (Figure 8). Site T5 which is located in a 8-membered ring perpendicular to the crystallographic axis c, has one eigenvector along z, and the two others perpendicular to z. Eigenvectors associated with the passes, are also arranged according to the local symmetry and the bonding pattern. When the Si-O-Si bond is linear, one eigenvector is aligned with the oxygen-silicon bond, and the two others are consequently perpendicular to that chemical bond. If the pass is located on a local symmetry element, *e.g.*, at positions between T1 and T2, or between T5 and T6

Table 4. *Peak properties (orthonormal eigenvectors components in gu) of ferrierite and mordenite electron density maps at 3 Å resolution.*

	First eigenvector (gu) [a]	Second eigenvector (gu)	Third eigenvector (gu)
Ferrierite			
T1	0.137	0.990	0.018
	-0.008	-0.017	0.998
	0.991	-0.137	0.006
T2	0.987	0.014	-0.160
	-0.161	-0.005	-0.987
	-0.015	0.999	-0.003
T3	0.723	-0.690	0.008
	-0.004	0.008	0.999
	-0.690	-0.724	0.003
T4	0.614	-0.734	0.290
	0.053	-0.328	-0.943
	0.787	0.595	-0.162
Mordenite			
T1	0.228	0.391	0.892
	-0.946	-0.127	0.298
	0.230	-0.911	0.341
T2	-0.229	-0.391	0.892
	0.946	0.126	0.298
	-0.229	0.912	0.341
T3	0.992	-0.121	-0.029
	0.124	0.985	0.118
	0.015	-0.121	0.993
T4	0.992	0.122	-0.029
	-0.125	-0.985	0.118
	-0.014	0.121	0.993
T5	0.997	0.077	0.009
	-0.077	0.997	-0.003
	-0.009	0.002	1.000
T6	-0.794	0.608	0.020
	-0.603	-0.793	-0.015
	0.007	-0.024	1.000

[a] gu = "grid unit", i.e., *grid interval.*

in mordenite, one of the eigenvector bissects the Si-O-Si angle (Figure 8). The analysis of Tables 3 and 4 shows that sites T1 and T2, as well as T3 and T4 present the same topological properties. This can be explained if it is considered that the space group of mordenite framework is Cmcm, a higher symmetry group than Cmc21 which is reported in the MSI database. In such symmetry conditions, T1 and T3 are equivalent to T2 and T4, respectively.

As shown by equation (7), the eigenvector orientations are explicitly considered in the calculation of the connection weights. Connections determined between peaks and passes of 3 Å resolution EDMs are displayed in Figures 5 and 6 for ferrierite and mordenite, respectively. They were obtained by imposing a maximal cutoff value to Δr (2.5 Å) and F (3 – cos30° – cos30°). Bond weight distributions that were obtained from the statistical analysis of connections within one asymmetric unit are described in Table 5. It is first observed that standard deviation values are an order of magnitude smaller for R and $F_{i\ or\ j}$ distributions than for w_{ij} and Δr. These two last distributions are actually composed of two distinct regions (Figures 9 and 10) whose unique origin comes from the short- and long-range order of the crystalline zeolitic frameworks. Indeed, in such cases, it is very easy to choose maximal cutoff values for Δr and F because of the discontinuity in their distributions. Second, F_i is not smaller than 0.75 for ferrierite and 0.73 for mordenite. These values correspond to angle values of 41 and 43 degrees. Considering the selected cutoff value for F, this implies that F_j is equal to 1.00, *i.e.*, there is a perfect alignement of the eigenvector associated with critical point j with the interdistance vector.

Shape analysis

Starting from equation (10), ellipsoid radii were calculated for each peak, *i.e.*, for each tetrahedral site. Their values, in grid units (gu) and in Å, are reported in Table 6. The resulting ellipsoid representation is displayed in Figures 11 and 12 which were obtained by displacing a probe (radius = 0. Å) on a regular grid and evaluating whether it enters (E_{ij} = 99) or not (E_{ij} = 0) an ellipsoid. Ellipsoids are visualized using an iso-energy contour of 90 (arbitrary units). Re-entering each radius value (in gu) together with its corresponding eigenvalue h (in e^-/gu^2 Å^3) in equation (8) allowed the evaluation of surface density value. For ferrierite, ellipsoids T1, T2, T3, and T4 (Figure 11) are characterized by a surface density equal to 0.98, 0.83, 0.93, and 0.89 $e^-/Å^3$, respectively, while

Table 5. *Description of the connection weight distributions w_{ij} and their contributions (Δr, R, $F_{i\ or\ j}$) (see equation 7) calculated from a critical point analysis of ferrierite and mordenite electron density maps at 3 Å resolution.*

	Min.	Max.	Mean	Standard Deviation
Ferrierite				
$\mathbf{w_{ij}}$	0.83	1.27	0.98	0.13
Δr (Å)	1.45	1.81	1.61	0.10
R	0.50	0.61	0.54	0.03
$\mathbf{F_{i\ or\ j}}$	0.75	1.00	0.94	0.07
Mordenite				
$\mathbf{w_{ij}}$	0.72	1.26	0.97	0.13
Δr (Å)	1.44	1.70	1.58	0.07
R	0.49	0.62	0.53	0.03
$\mathbf{F_{i\ or\ j}}$	0.73	1.00	0.93	0.09

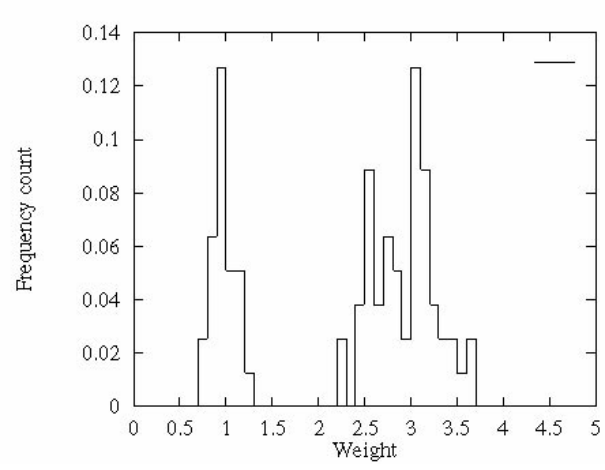

Figure 9. *Frequency distribution of connection weight values (w_{ij}) obtained from the critical point analysis of the mordenite electron density map at 3 Å resolution.*

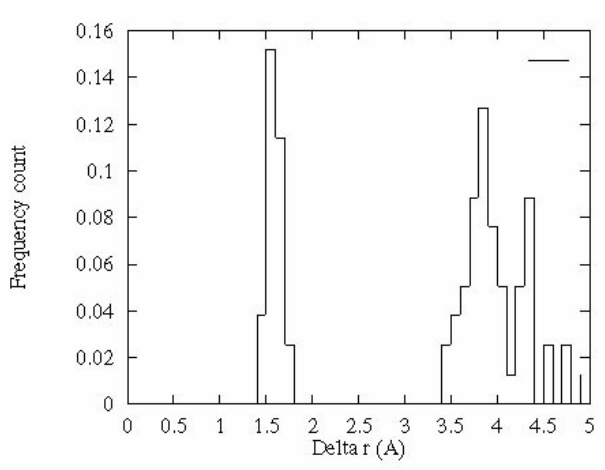

Figure 10. *Frequency distribution of connection lengths (Δr) obtained from the critical point analysis of the mordenite electron density map at 3 Å resolution.*

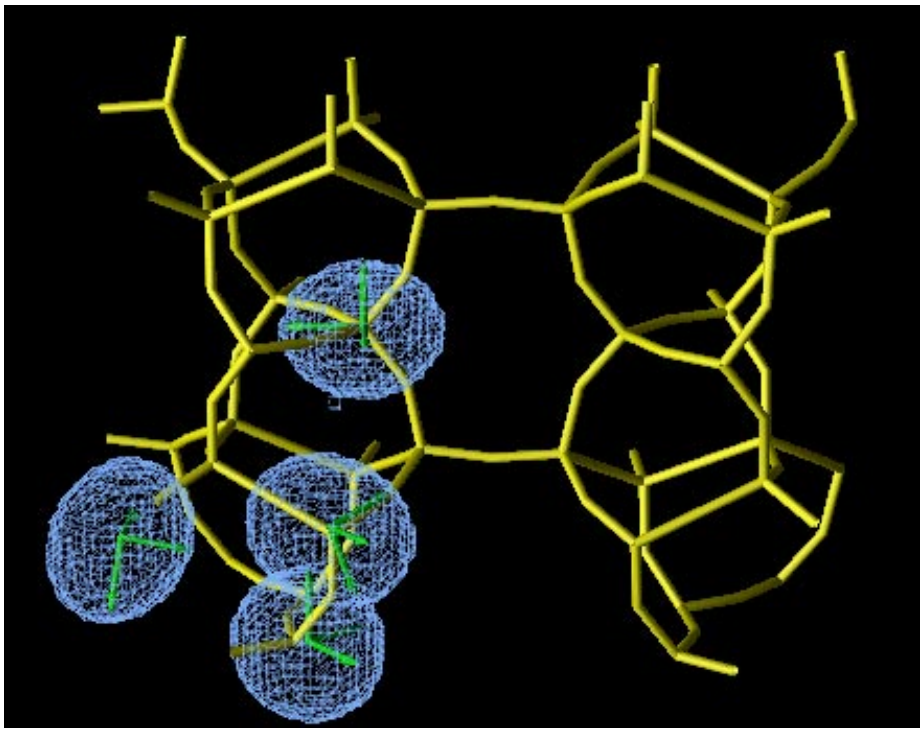

Figure 11. *Ellipsoids built on the peaks associated with the four tetrahedral sites of ferrierite obtained from the topological analysis of the 3 Å resolution electron density map. The results are superimposed onto the crystallographic structure (yellow sticks) retrieved from the MSI Technologies data bank. Length of eigenvectors (green arrows) is set equal to the respective ellipsoid radius value.*

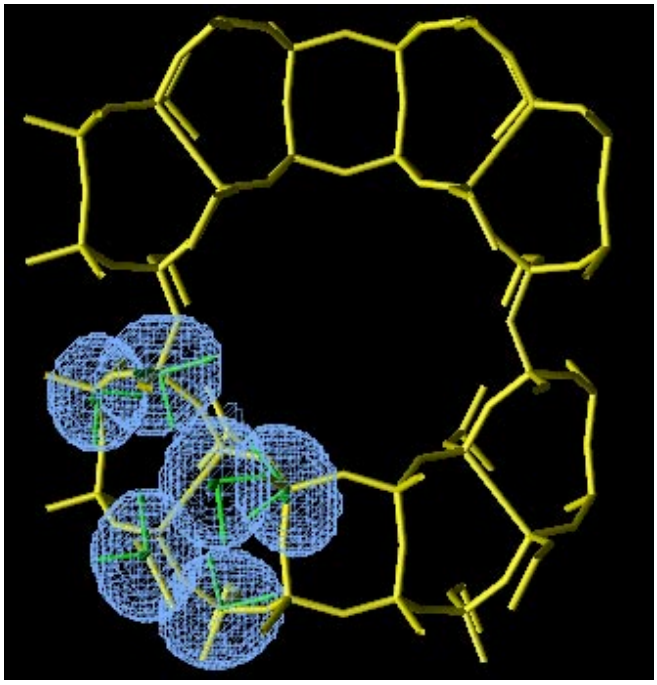

Figure 12. *Ellipsoids built on the peaks associated with the six tetrahedral sites of mordenite obtained from the topological analysis of the 3 Å resolution electron density map. The results are superimposed onto the crystallographic structure (yellow sticks) retrieved from the MSI Technologies data bank. Length of eigenvectors (green arrows) is set equal to the respective ellipsoid radius value.*

in the case of mordenite (Figure 12), each individual T-site is defined by a surface density equal to 0.85, 0.85, 0.87, 0.87, 0.89, and 0.86 $e^{-}/Å^3$. This thus shows that a contour defined by the set of all ellipsoid surfaces does not correspond to a unique iso-electron density contour: the ellipsoid surface density values depend on the peak height. Figures 13 and 14 illustrate the fit between the ellipsoid surfaces and the electron density contours. Ellipsoid boundaries (red contours) and iso-electron density surfaces were drawn on a plane crossing the ferrierite structure at z = c/2 (Figure 13), and mordenite at z = 0 (Figure 14). From these figures, it is concluded that the ellipsoid representation is a good first approximation of the shape of the zeolite structure. It is defined by a reduced number of parameters, peak heights, and Hessian matrices, rather than by a three-dimensional grid of points. However, such a model of a continuous 3D function allows discontinuities (cusps) to appear on the molecular surface. Fortunately, this do not raise any problem when the approximation model serves as a basis for pseudo- pair-wise interaction energy calculations. It is interesting at this level to note the presence of unphysical density maxima, or ripples, in the centre of the zeolite cavities. They are easily observed in Figure 13, at the bottom right corner of the iso-contours box. Thus, modeling the zeolite structure using well-selected ellipsoids is a way to avoid the presence of these unphysical objects in interaction energy evaluations.

Interaction energy calculation

As presented in the Methodology, calculation of pseudo-interaction energy values between the framework and a probe

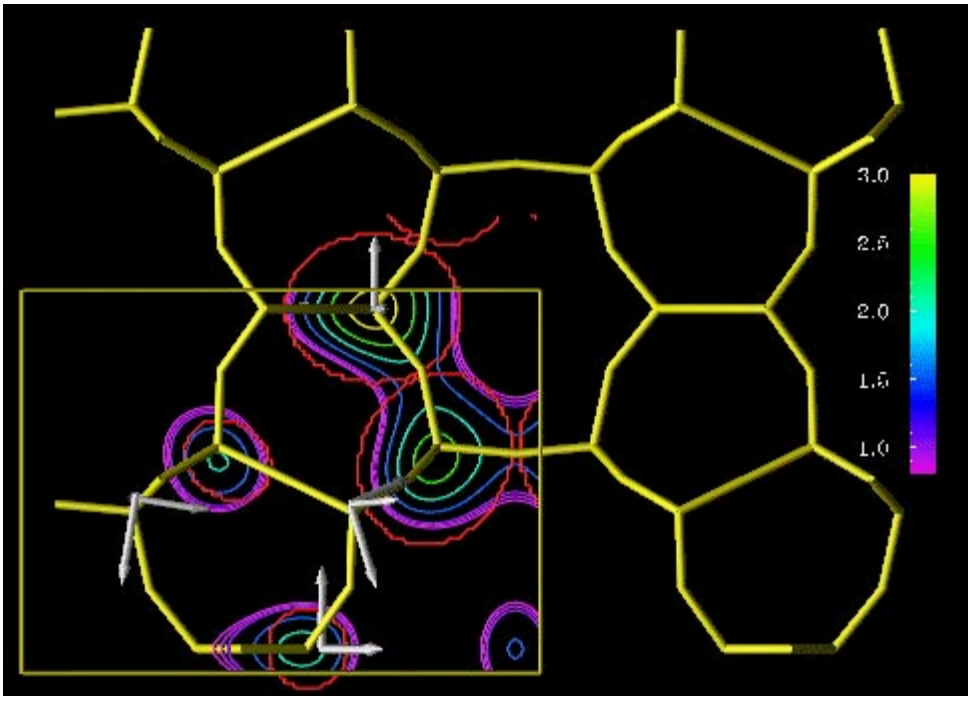

Figure 13. *Ellipsoids surface contour (E = 90 in arbitrary units) built on the peaks associated with the tetrahedral sites of ferrierite obtained from the topological analysis of the 3 Å resolution electron density map (iso-electron density contours are displayed in the plane z = c/2: 0.8, 0.9, 1.0, 1.5, 2.0, and 2.5 $e^-/Å^3$). The results are superimposed onto the crystallographic structure (yellow sticks) retrieved from the MSI Technologies data bank. Eigenvectors are shown using white arrows.*

can be achieved through a Lennard-Jones type expression. We have selected different probe sizes ranging between 1.6 and 2.2 Å; major changes in the potential energy topography were observed when the probe size was increased from 1.9 to 2.0 Å. Results obtained with these parameters are displayed in Figures 15-18. T-site multiplicity was considered in order to avoid multiple energy counts.

Energy results for ferrierite interacting with the smallest probe (r = 1.9 Å) are presented in Figure 15 as 3-dimensional iso-energy surfaces and 2-dimensional iso-energy contours displayed in plane x = a/2. The figure allows the visualization of the density contours along the 10- (bottom central channel) and 8-membered ring channels. Translational motion is permitted along the channels wherein attractive energy wells are observed nearby the internal surfaces. Fig-

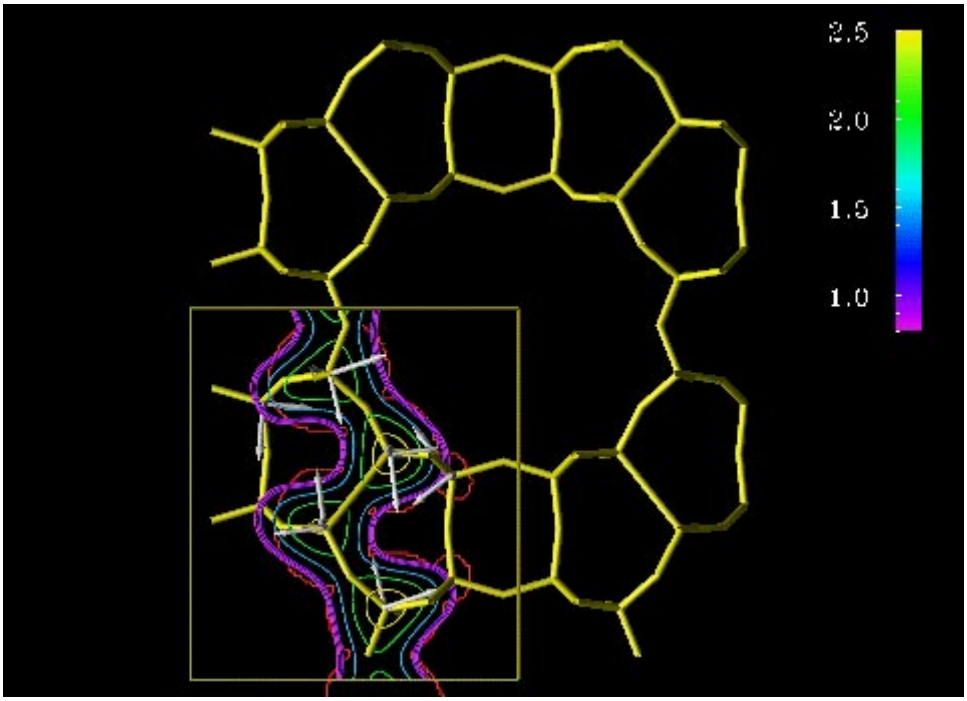

Figure 14. *Ellipsoids surface contour (E = 90 in arbitrary units) built on the peaks associated with the tetrahedral sites of mordenite obtained from the topological analysis of a 3 Å resolution electron density map (iso-electron density contours are displayed in the plane z = 0: 0.8, 0.9, 1.0, 1.5, 2.0, 2.5, and 3.0 $e^-/Å^3$). The results are superimposed onto the crystallographic structure (yellow sticks) retrieved from the MSI Technologies data bank. Eigenvectors are shown using white arrows.*

Table 6 *Peak properties (radii) of ferrierite and mordenite electron density maps at 3 Å resolution.*

	r1 [gu] (Å)	r2 [gu] (Å)	r3 [gu] (Å)
Ferrierite			
T1	[10.55] (1.65)	[10.96] (1.87)	[12.49] (1.58)
T2	[9.41] (1.60)	[12.80] (2.00)	[14.57] (1.86)
T3	[9.74] (1.60)	[11.65] (1.90)	[14.15] (1.79)
T4	[10.35] (1.67)	[11.05] (1.78)	[14.54] (1.91)
Mordenite			
T1	[9.74] (1.76)	[10.65] (1.68)	[12.23] (1.99)
T2	[9.73] (1.76)	[10.65] (1.68)	[12.23] (1.99)
T3	[9.79] (1.58)	[10.43] (1.90)	[12.26] (1.93)
T4	[9.79] (1.59)	[10.43] (1.90)	[12.27] (1.93)
T5	[9.38] (1.52)	[9.84] (1.80)	[12.58] (1.97)
T6	[9.06] (1.54)	[11.27] (1.98)	[12.48] (1.96)

ure 15 also shows that translational motion of the probe across 6-membered windows is feasible only through an energy barrier of about 1 (in arbitrary units). It was also observed that this barrier appears for probes with a radius larger than 1.6 Å. The centre of cavities sandwiched between two facing 6-membered rings does not correspond to a potential energy well (bottom left and right of Figure 15) and the probe seems to be preferentially physisorbed close to the cavity internal walls.

Similar representations for the larger probe (r = 2.0 Å) interacting with ferrierite are shown in Figure 16. Translation along 10-T channels is still possible (bottom central channel), but is now observed that iso-contours of potential energy wells are located in the centre of this kind of channels, rather than along the walls. In this context, the large probe is viewed as a 'floating' atom while the small one adopts the behaviour of a 'creeping' atom [38]. A creeping-like character still appears in cavities limited by two 6-T windows (bottom left and right of Figure 16).

Mordenite-probe iso-energy contours are shown in Figures 17 and 18 in planes x = 0 (left plane) and x = a/2 (right plane). Both probes (r = 1.9 and 2.0 Å) have a rather floating behaviour along the main 12-T channels (centre of plane x = a/2). However, due to confinement effects, more attractive energies are observed inside the lateral pockets linking the 12-T channels together. Translation along these pockets is energetically feasible for the smallest probe through a zig-zag path (Figure 17) while it is forbidden for the largest one (Figure 18). These results are perfectly compatible with previous conventional molecular mechanics calculations [23] that were carried out for Ne (critical radius = 1.6 Å) and Xe (critical radius = 2.185 Å) in mordenite using a Lennard-Jones type potential. However, these comparisons must be considered with caution since our probes should be seen as the result of a critical point analysis of a 3 Å electron density map.

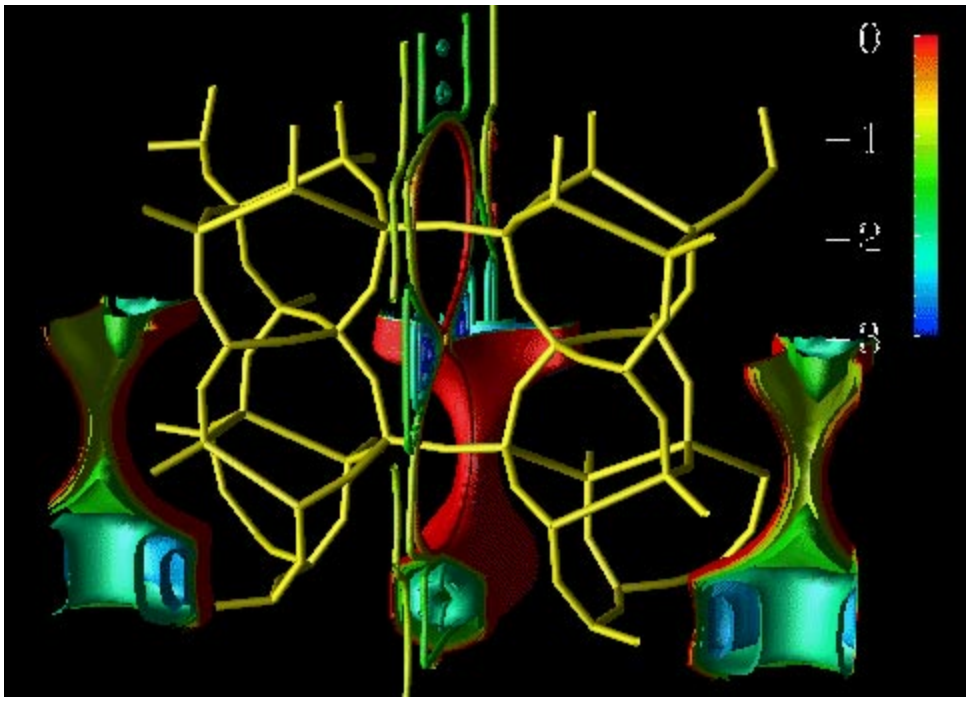

Figure 15. *Ferrierite-probe (r = 1.9 Å) interaction energy iso-contours (from -3.0 to 0.0, step = 0.5 in arbitrary units) calculated from a critical point representation obtained from the topological analysis of an electron density map at 3 Å resolution. 2D iso-energy contours are displayed in plane x = a/2. The results are superimposed onto the crystallographic structure (yellow sticks) retrieved from the MSI Technologies data bank.*

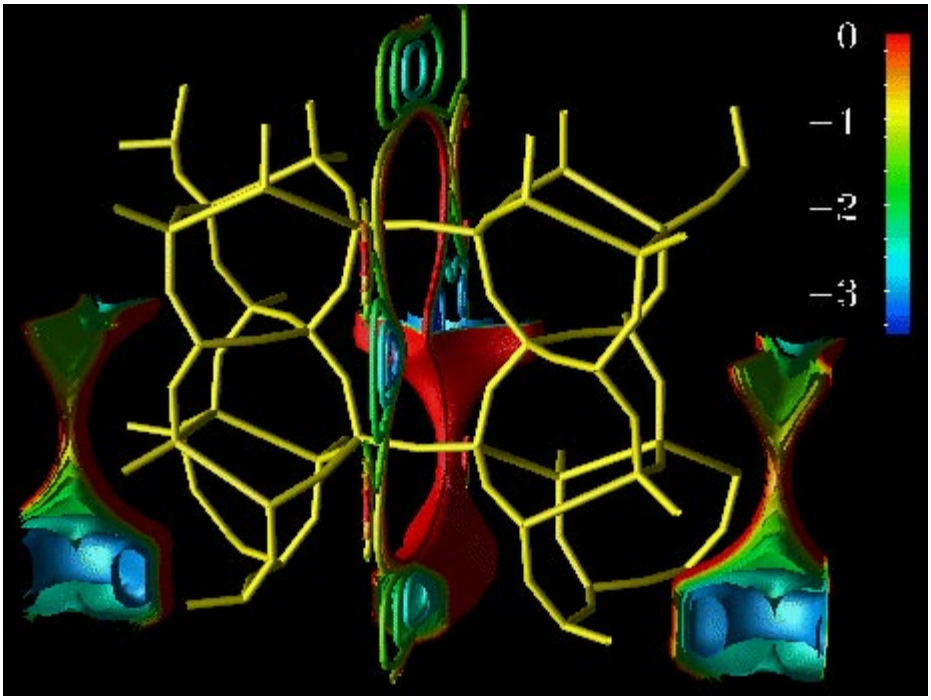

Figure 16. *Ferrierite-probe (r = 2 Å) interaction energy iso-contours (from –3.5 to 0.0, step = 0.5 in arbitrary units) calculated from a critical point representation obtained from the topological analysis of an electron density map at 3 Å resolution. 2D iso-energy con-tours are displayed in planex = a/2. The results are superimposed onto the crystallographic structure (yellow sticks) retrieved from the MSI Technologies data bank.*

Conclusions

We have presented a critical point analysis method derived from the initially implemented code by C.K. Johnson. It was applied to shape analysis of ferrierite and mordenite electron density maps at 3 Å resolution. It was observed that the 3D crystalline arrangement of silicon and oxygen atoms generated peaks on the tetrahedral sites, and passes very close to the oxygen atoms. The linkage between these critical points was determined through the calculation of connection weights whose range of acceptable values is easily defined due to the short- and long-range order of the crystalline structures. Consequently, a zeolite structure can be fully reconstructed from the topological analysis of its medium resolution electron density maps. We have also shown that fitting ellipsoids on each local density maximum (peaks) allowed to reconstruct

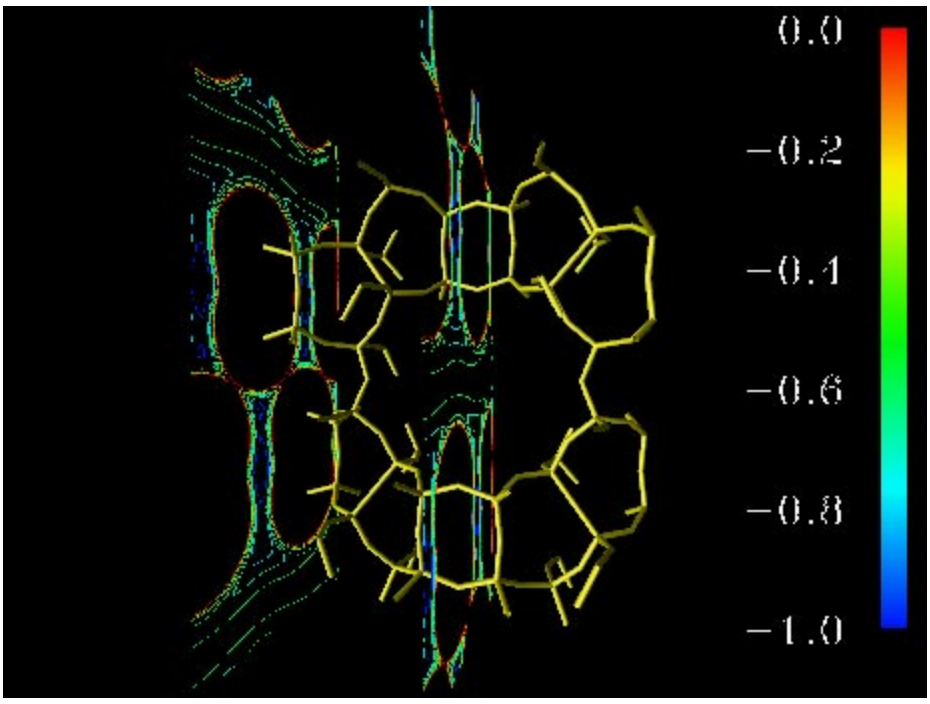

Figure 17. *Mordenite-probe (r = 1.9 Å) interaction energy iso-contours (from –1.0 to 0.0, step = 0.2, and -0.7 in arbitrary units) displayed in planes x = 0 (left plane) and x = a/2 (right plane), calculated from a critical point representation obtained from the topological analysis of an electron density map at 3 Å resolution. The results are superimposed onto the crystallographic structure (yellow sticks) retrieved from the MSI Technologies data bank.*

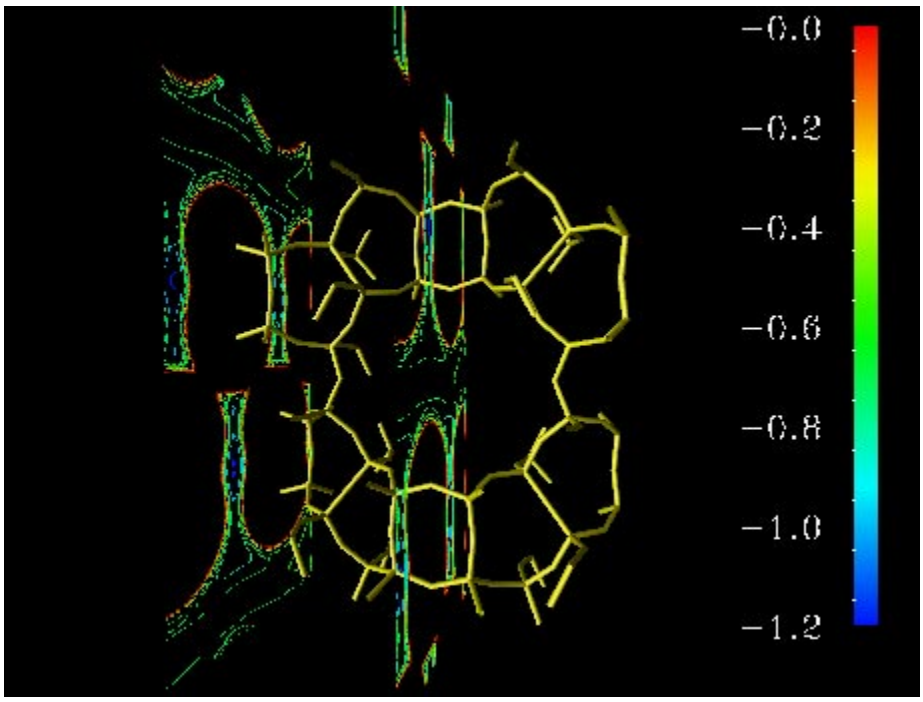

Figure 18. *Mordenite-probe (r = 2 Å) interaction energy iso-contours (from –1.2 to 0.0, step = 0.2, and -0.7 in arbitrary units) displayed in planes x = 0 (left plane) and x = a/2 (right plane), calculated from a critical point representation obtained from the topological analysis of an electron density map at 3 Å resolution. The results are superimposed onto the crystallographic structure (yellow sticks) retrieved from the MSI Technologies data bank.*

the zeolite shape and to evaluate steric interaction energies between the framework and a spherical probe.

The work that is presented assesses the potentialities of a critical point analysis method in the field of shape analysis at medium resolution. Besides very important advantages, it has shown some limitations, but also new potential applications. Advantages consist in the simplification of 3D electron density (ED) grids into graphs composed of a limited number of critical points and their properties (density value and eigenvalues). These properties allow the local reconstruction of the anisotropic ED distribution through ellipsoid assignment to peaks. The evaluation of steric interaction energies with a molecular probe can consequently be performed. To those advantages correspond some limitations. Due to ellipsoid reconstruction, the smoothness of ED maps is lost and energies are given in arbitrary units. Regarding this second consequence, we are trying to determine how contributions such as electrostatic energies could be added to the steric interaction potential that was obtained in the present work. However, new applications of our method can already be considered, especially regarding the evaluation of steric interaction energies. Rather than probing an empty framework with a spherical element, it would be very interesting to generate an ED map of the zeolite already interacting with a molecule, and to determine how its topological representation is affected by the interacting molecule.

In summary, this work reports our very first attempts to apply a new method to the evaluation of interactions between small molecules in highly confined environments. It is clear that conventional interaction potentials (Lennard-Jones) provide quantitative energy results; hence their large use in molecular modeling and molecular simulation methods. With respect to these classical approaches, our method presents a major difference: the number of elements to be considered to model the zeolitic framework is reduced (the number of peaks is lower than the number of atoms) but the shape (orientation) of these elements, which is related to their environment, is considered. We expect this shape component to be a variable depending upon the chemical nature of the zeolite and the guest molecule, since it is derived from electron density properties. Further calculations will be carried out to verify how topological properties are affected by the nature of the sorbed molecule and by a change in the chemical composition of the framework, *e.g.*, acidic sites. We expect that our approach is able to complete the representation of zeolite structures in databases, by associating new descriptive parameters with their basic tetrahedral sites. We also wish to carry out topological analyses of the generated 3D potential energy map in order to predict the size and orientation of possible guest molecules within the zeolitic framework.

Acknowledgments. All authors wish to thank C.K. Johnson for providing the program ORCRIT, S. Fortier, J.I. Glasgow, and F.H. Allen for fruitful discussions, and the FUNDP for the use of the Namur Scientific Computing Facility (SCF) Center. They also acknowledge the financial support of the FNRS-FRFC, the "Loterie Nationale" for the convention no 9.4593.92, the FNRS within the framework of the "Action d'impulsion à la recherche fondamentale" of the Belgian Ministry of Science under the convention no. D.4511.93., and IBM-Belgium for the Academic Joint Study on "Cooperative Processing for Theoretical Physics and Chemistry". LL thanks the FNRS for her "Chargée de Recherches" position.

References

1. Norel, R.; Fisher, D.; Wolfson, H.J.; Nussinov, R. *Protein Engineering* **1994**, *7*, 39.
2. Mezey, P.G. in Johnson, M.A.; Maggiora, G.M. (Eds.) *Concepts and Applications of Molecular Similarity* J. Wiley & Sons: New York, **1990**, p. 321.
3. Mezey, P.G. *J. Comput. Chem.* **1987**, *8*, 462.
4. Arteca, G.A.; Mezey, P.G. *J. Comput. Chem.* **1988**, *9*, 608.
5. Lin, S.L; Nussinov, R.; Fisher, D.; Wolfson, H.J., *PROTEINS: structure, functions and genetics* **1994**, *18*, 94.
6. Bader, R.W. *Atoms in Molecules - A Quantum Theory*; Clarendon: Oxford, 1990.
7. Johnson, C.K. ORCRIT - The Oak Ridge Critical Point Network Program; Oak Ridge National Laboratory: Oak Ridge, **1977**.
8. Greer, J. *J. Mol. Biol.* **1974**, *82*, 279; ibid. *J. Mol. Biol.* **1975**, *98*, 649; ibid. *J. Mol. Biol.* **1976**, *100*, 427; ibid. *J. Mol. Biol.* **1976**, *104*, 371.
9. Jones, T.A. *J. Applied Cryst.* **1978**, *11*, 268; Jones, T.A.; Zou, J.Y.; Cowan, S.W.; Kjeldgaard, M. *Acta Cryst. A* **1991**, *47*, 110.
10. Fortier, S.; Castleden, I.; Glasgow, J.; Conklin, D.; Walmsley, C.; Leherte, L.; Allen, F.H. *Acta Cryst. D* **1993**, *49*, 168.
11. Leherte, L.; Fortier, S.; Glasgow, J.; Allen, F.H. *Acta Cryst. D* **1994**, *50*, 155.
12. *Proceedings of the Second International Conference on Intelligent Systems for Molecular Biology;* Leherte, L.; Baxter, K.; Glasgow, J.; Fortier, S. in Altman, R.; Brutlag, D.; Karp, P.; Lathrop, R.; Searls, D., Eds. MIT/AAAI: Menlo Park, 1994; p. 261.
13. Shirsat, R.N.; Bapat, S.V.; Gadre, S.R. *Chem. Phys. Lett.* **1992**, *200*, 373.
14. Gadre, S.R., Pundlik, S.S. *J. Amer. Chem. Soc.* **1995**, *117*, 9559.
15. Wild, D.J.; Willett, P. *J. Chem. Inf. Comput. Sci.* **1996**, *36*, 159.
16. Thorner, D.A.; Wild, D.J.; Willett, P.; Wright, P.M. *J. Chem. Inf. Comput. Sci.*, **1996**, *36*, 900.
17. Good, A.C.; Hodgkin, E.E.; Richards, W.G. *J. Chem. Inf. Comput. Sci.* **1992**, *32*, 188.
18. Good, A.C.; Richards, W.G. *J. Chem. Inf. Comput. Sci.* **1993**, *33*, 112.
19. Lee, C.; Smithline, S. *J. Phys. Chem.* **1994**, *98*, 1135.
20. Grant, J.A.; Pickup, B.T. *J. Phys. Chem.* **1995**, *99*, 3503.
21. Mestres, J.; Sola, M.; Duran, M.; Carbo, R. *J. Comput. Chem.* **1994**, *15*, 1113.
22. Carbo, R.; Calabuig, B.; Vera, L.; Besalu, E. *Adv. Quantum Chem.* **1994**, *25*, 253.
23. Derouane, E.G.; Leherte, L.; Vercauteren, D.P.; Lucas, A.A.; André, J.-M. *J. Catal.* **1989**, *119*, 266.
24. Liotard, D.; Rérat, M. *Theor. Chim. Acta* **1993**, *86*, 297.
25. Birkhoff, G.; Cavendish, J.C.; Gordon, W.J. *Proc. Natl. Acad. Sci. USA* **1974**, *71*, 3423.
26. Vetterling, W.T.; Teukolsky, S.A.; Press, W.H.; Flannery, B.P. *Numerical Recipes* Cambridge University: Cambridge, 1989.
27. Shoichet, B.; Kuntz, I.D. *Protein Engineering* **1993**, *6*, 723.
28. Grootenhuis, P.D.J.; Roe, D.C.; Kollman, P.A., Kuntz, I.D. *J. Comput. Aided Mol. Design* **1994**, *8*, 731.
29. Good, A.C.; Ewing, T.J.A.; Gschwend, D.A.; Kuntz, I.D. *J. Comput. Aided Mol. Design* **1995**, *9*, 1.
30. Derouane, E.G.; B.Nagy, J.; Fernandez, C.; Gabelica, Z.; Laurent, E.; Maljean, P. *Appl. Catal. Lett.* **1988**, *40*, L1.
31. Derouane, E.G.; Vanderveken, D.J. *Appl. Catal.* **1988**, *45*, L15.
32. Derouane, E.G. In *Guidelines for Mastering the Properties of Molecular Sieves;* Barthomeuf, D.; Derouane, E.G.; Hölderich, W., Eds.; Plenum: New York, 1990; p. 225.
33. InsightII graphics interface, version 3.0.0, Molecular Simulation Inc., San Diego, 1996.
34. Xtal3.0 Reference Manual, Hall, S.R.; Stewart, J.M., Eds.; Universities of Western Australia and Maryland; Lamb: Perth, 1990.
35. Leherte, L.; Allen, F.H. *J. Comput. Aided Mol. Design* **1994**, *8*, 257.
36. Leherte, L.; Latour, Th; Vercauteren, D.P. *Supramolecular Science* **1995**, *2*, 209.
37. Leherte, L.; Latour, Th.; Vercauteren, D.P. *J. Comput. Aided Mol. Design* **1996**, *10*, 55.
38. Derouane, E.G.; André, J.-M.; Lucas, A.A. *J. Catal.* **1988**, *110*, 58.